

## Supplementary material to the paper:

## Complex refractive indices and single scattering albedo of global dust aerosols in the shortwave spectrum and relationship to iron content and size

Claudia Di Biagio<sup>1</sup>, Paola Formenti<sup>1</sup>, Yves Balkanski<sup>2</sup>, Lorenzo Caponi<sup>1,3</sup>, Mathieu Cazaunau<sup>1</sup>, Edouard Pangui<sup>1</sup>, Emilie Journet<sup>1</sup>, Sophie Nowak<sup>4</sup>, Meinrat O. Andreae<sup>6,12</sup>, Konrad Kandler<sup>7</sup>, Thuraya Saeed<sup>8</sup>, Stuart Piketh<sup>9</sup>, David Seibert<sup>10</sup>, Earle Williams<sup>11</sup>, and Jean-Francois Doussin<sup>1</sup>

Correspondence to: C. Di Biagio ([claudia.dibiagio@lisa.u-pec.fr](mailto:claudia.dibiagio@lisa.u-pec.fr))

## Calculation of the size distribution behind SW instruments inlets

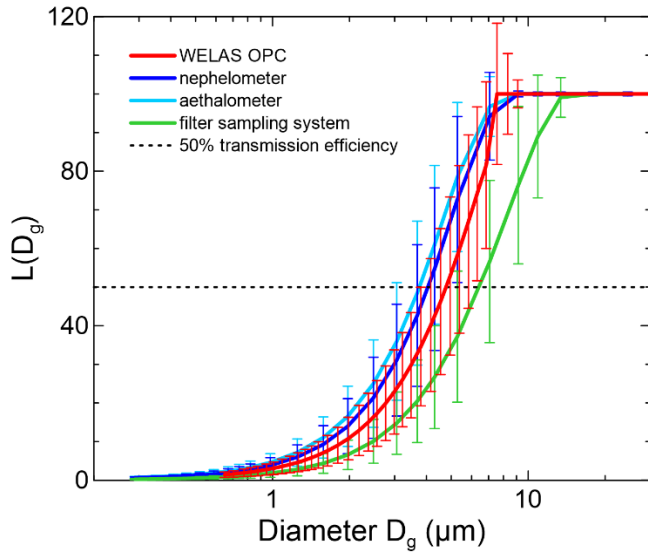
The size distribution sensed by SW optical instruments, i.e. that behind the SW optical instruments inlets ( $dN/d\log D_g|_{SW\text{optics}}$ ), was calculated started from the size in CESAM. To do so, the particle loss functions in the sampling lines for the nephelometer and the aethalometer were calculated as a function of particle diameter ( $L_{\text{neph}}(D_g)$ ,  $L_{\text{aeth}}(D_g)$ ) using the Particle Loss Calculator (PLC, von der Weiden et al., 2009) using as input the geometry of the sampling line, the sampling flow rate, the particle shape factor, and the particle density. The uncertainty on calculated loss functions was estimated with a sensitivity study by varying in the PLC software values of the input parameters within their estimated uncertainties.

As shown in Fig. S1, the loss functions agree within uncertainties for the nephelometer and the aethalometer in the entire diameter range, meaning that the same dust size distribution is sensed by the two instruments. An average loss function ( $L_{SW\text{optics}}(D_g)$ ) between that of the nephelometer and the aethalometer was calculated and used to estimate a common  $(dN/d\log D_g)_{SW\text{optics}}$  as:

$$\left[ \frac{dN}{d\log D_g} \right]_{SWoptics} = \left[ \frac{dN}{d\log D_g} \right]_{CESAM} (1 - L_{SWoptics}(D_g)) \quad (1).$$

34 **Fig S1.** Particle loss function versus particle geometric diameter ( $L(D_g)$ ) calculated for the WELAS OPC,  
 35 the nephelometer, the aethalometer, and the filter sampling inlets by using the Particle Loss Calculator  
 36 software (von der Weiden et al., 2009). The uncertainty on calculated loss functions was estimated with  
 37 a sensitivity study by varying in the PLC software values of the input parameters within their estimated  
 38 uncertainties.

39



40

41

42

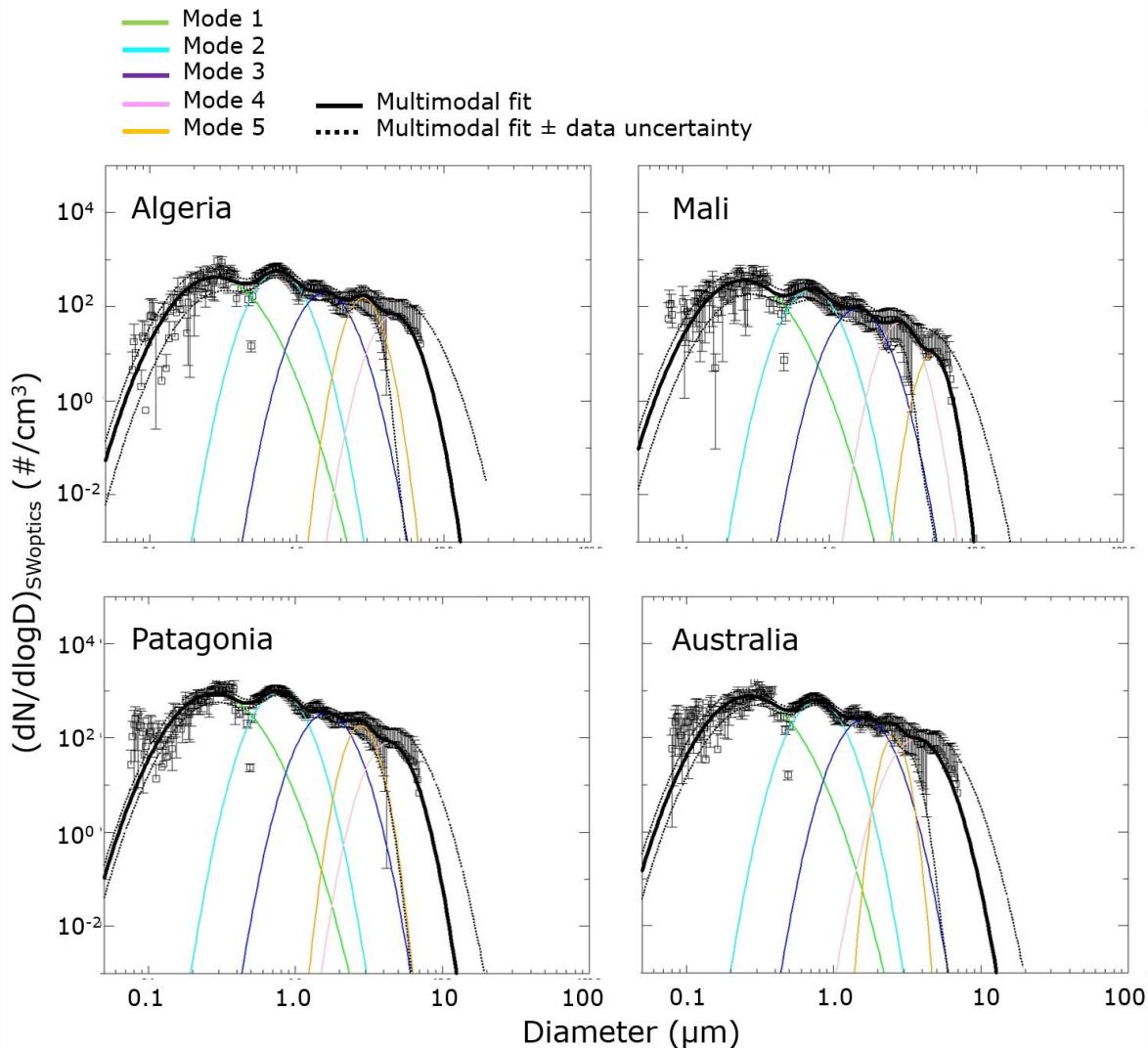
#### 43 **Lognormal fitting parameters of the dust size distribution**

44 The dust size distribution ( $dN/d\log D$ )<sub>SWoptics</sub> measured at each 10-min time step for each sample was  
 45 fitted with a sum of five lognormal functions. For each mode the parameters of the lognormal functions,  
 46 i.e. the total number concentration ( $N_i$ ), the geometric median diameter ( $D_{g,i}$ ), and the geometric  
 47 standard deviation of the distribution ( $\sigma_i$ ), were retrieved. The uncertainty on the retrieved parameters  
 48 were estimated by repeating the fits by using size data within their uncertainties. The central parameters  
 49 of the lognormal fitting of ( $dN/d\log D_g$ )<sub>SWoptics</sub> at the peak of the injection are reported in Table S1 while  
 50 an example of the multimodal fit for four dust samples are shown in Fig. S2. The average geometrical  
 51 diameter and standard deviation for the five modes are very similar between the nineteen different  
 52 samples, so that the same modes contribute to the dust size. The relative proportion of the modes  
 53 nonetheless largely changes from sample to sample, suggesting that different soils are more or less  
 54 prone to generate different aerosol size fractions. It also changes with time for each given sample, in  
 55 particular with the decrease of the largest modes due to gravitational settling in the chamber. The time–  
 56 and sample–averaged  $D_g$  and  $\sigma$  ( $\pm$  their st.dev.) of the five modes are 0.26 ( $\pm$ 0.04) and 1.53 ( $\pm$ 0.08) for  
 57 mode 1, 0.71 ( $\pm$ 0.05) and 1.31 ( $\pm$ 0.04) for mode 2, 1.47 ( $\pm$ 0.11) and 1.30 ( $\pm$ 0.02) for mode 3, 2.56  
 58 ( $\pm$ 0.26) and 1.17 ( $\pm$ 0.06) for mode 4, and 3.77 ( $\pm$ 0.53) and 1.25 ( $\pm$ 0.08) for mode 5. Note that the fit of  
 59 field observations also usually requires four or five modes between 0.05 and 5.0  $\mu\text{m}$  geometrical  
 60 diameter (e.g., Osborne et al., 2008; Ryder et al., 2013a; Denjean et al., 2016a).

61

62

63 **Figure S2.** Example of multimodal lognormal fitting for four dust size distribution datasets measured  
 64 behind the SW inlets during experiments with the Algeria, Mali, Patagonia, and Australia samples.  
 65 Shown data are 10-min average data taken 20 minutes after dust aerosol injection in the CESAM  
 66 chamber. The single modes contributing to the multimodal fit are shown in color. The multimodal fit  
 67 obtained as the sum of the single modes is also shown (thick black line) together with the multimodal  
 68 fits obtained by fitting data within plus or minus their error bars (dotted black lines). Fitted function were  
 69 cut at 10  $\mu\text{m}$  of diameters (the cutoff of the SW inlets) for subsequent utilization.



70

71

72

73

74

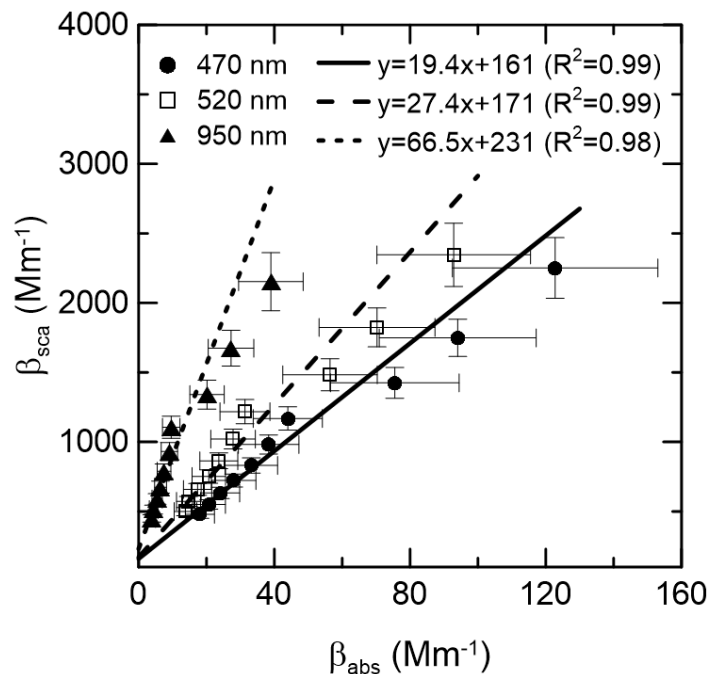
75

76

77

78 **Figure S3.** Example of correlation between scattering and absorption coefficients measured at the  
 79 wavelengths of 470, 520, and 950 nm for Morocco dust sample. The linear fits are also shown, and the  
 80 retrieved parameters of the fit and correlation coefficient ( $R^2$ ) are also indicated in the plot.

81



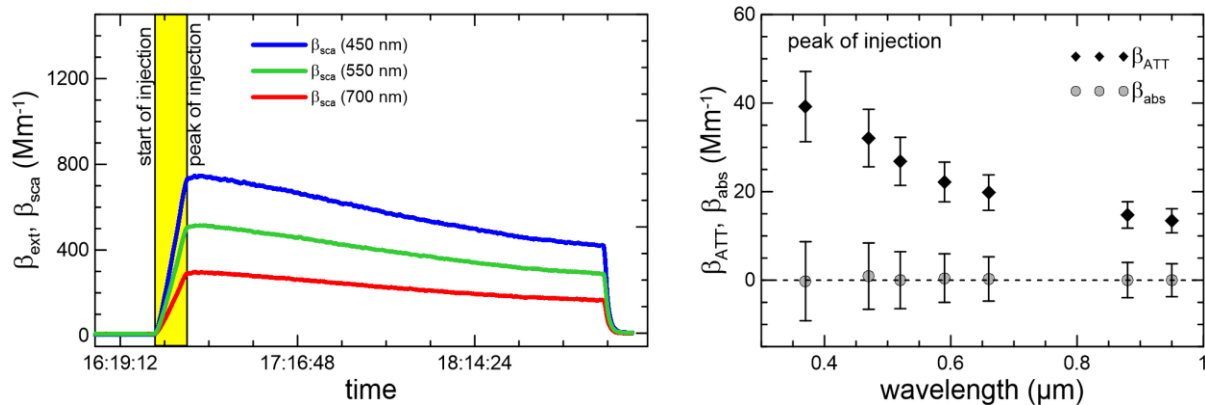
82

83

84 **Figure S4.** Control experiment with ammonium sulphate particles. Left panel: temporal evolution of the  
 85 scattering ( $\beta_{\text{sca}}$ ) coefficient measured in the chamber by the nephelometer at 450, 550, and 700 nm.  
 86 Right panel: spectral attenuation ( $\beta_{\text{ATT}}$ ) measured by the aethalometer and derived absorption  
 87 coefficient ( $\beta_{\text{abs}}$ ) at the peak of ammonium sulfate particles injection.

88

89



90

91

92

93

94 **Table S1** Parameters (total number concentration  $N_i$ , in no.  $\text{cm}^{-3}$ , geometric median diameter  $D_{g,i}$  in  $\mu\text{m}$ ,  
 95 and geometric standard deviation  $\sigma_i$ ) for the five log-normal modes  $i$  used to parameterize the number  
 96 size distributions at the peak of the dust injection in CESAM for the different dust samples.

97

	Mode 1			Mode 2			Mode 3			Mode 4			Mode 5		
	N	$D_g$	$\sigma_i$												
Tunisia	1050	0.27	1.50	507	0.69	1.30	221	1.4	1.30	49	2.6	1.19	36	3.9	1.31
Morocco	342	0.28	1.50	260	0.75	1.30	104	1.5	1.30	54	2.8	1.23	13	4.8	1.20
Libya	527	0.27	1.50	445	0.73	1.30	158	1.5	1.30	23	2.4	1.11	67	3.3	1.29
Algeria	267	0.29	1.50	207	0.77	1.30	65	1.6	1.30	37	2.8	1.20	26	4.5	1.25
Mauritania	269	0.25	1.50	139	0.72	1.30	51	1.5	1.30	17	2.7	1.17	8	4.2	1.20
Niger	468	0.24	1.50	305	0.69	1.30	150	1.4	1.30	31	2.4	1.15	58	3.6	1.35
Mali	234	0.24	1.51	76	0.75	1.30	26	1.6	1.30	6	2.5	1.11	10	3.4	1.23
Bodélé	1967	0.34	1.50	828	0.85	1.30	319	1.7	1.30	129	2.8	1.19	189	4.3	1.35
Ethiopia	460	0.28	1.50	443	0.76	1.30	148	1.6	1.30	72	2.7	1.18	59	4.2	1.32
Saudi Arabia	652	0.29	1.50	440	0.79	1.30	102	1.7	1.30	4	2.0	1.30	61	3.3	1.31
Kuwait	283	0.24	1.56	126	0.71	1.30	50	1.5	1.30	19	2.8	1.19	10	4.3	1.35
Gobi	1061	0.25	1.50	456	0.67	1.30	161	1.4	1.30	28	2.6	1.17	23	3.9	1.31
Taklimakan	610	0.27	1.50	423	0.77	1.30	179	1.6	1.30	71	2.7	1.18	88	4.1	1.34
Arizona	1261	0.29	1.50	858	0.82	1.30	285	2.0	1.41	10	2.0	1.35	66	4.5	1.27
Atacama	1144	0.27	1.50	1278	0.78	1.30	514	1.6	1.30	149	2.6	1.17	142	3.8	1.30
Patagonia	526	0.27	1.50	353	0.78	1.30	113	1.7	1.30	47	2.8	1.20	28	4.5	1.25
Namib-1	665	0.29	1.50	394	0.79	1.30	124	1.7	1.30	52	2.9	1.17	57	4.2	1.32
Namib-2	496	0.26	1.50	291	0.77	1.30	76	1.7	1.30	21	2.6	1.13	34	3.7	1.30
Australia	483	0.27	1.50	224	0.79	1.30	77	1.6	1.30	23	2.6	1.13	35	3.8	1.30

98

99

100 **Table S2.** Ångstrom Absorption Exponent (AAE) calculated as the power-law fit of  $\beta_{\text{abs}}$  versus  $\lambda$   
 101 between 370 and 950 nm. Mean and standard deviations over experiments are reported for each soil.

102

Geographical area	Sample	AAE
Northern Africa – Sahara	Tunisia	$2.0 \pm 0.1$
	Morocco	$2.0 \pm 0.2$
	Libya	$2.2 \pm 0.1$
	Algeria	$2.3 \pm 0.4$
	Mauritania	$2.2 \pm 0.2$
Sahel	Niger	$1.7 \pm 0.1$
	Mali	$1.5 \pm 0.3$
	Bodélé	$2.3 \pm 0.1$
Eastern Africa and the Middle East	Ethiopia	$2.2 \pm 0.1$
	Saudi Arabia	$2.4 \pm 0.1$
	Kuwait	$2.3 \pm 0.3$
Eastern Asia	Gobi	$2.1 \pm 0.1$
	Taklimakan	$2.0 \pm 0.1$
North America	Arizona	$1.6 \pm 0.2$
South America	Atacama	$1.8 \pm 0.1$
	Patagonia	$2.2 \pm 0.4$
Southern Africa	Namib-1	$2.1 \pm 0.3$
	Namib-2	$2.0 \pm 0.2$
Australia	Australia	$2.2 \pm 0.2$

103

104 **References**

105 Denjean, C., Cassola, F., Mazzino, A., Triquet, S., Chevaillier, S., Grand, N., Bourrianne, T., Momboisse, G.,  
106 Sellegrí, K., Schwarzenböck, A., Freney, E., Mallet, M., and Formenti, P.: Size distribution and optical properties  
107 of mineral dust aerosols transported in the western Mediterranean, *Atmos. Chem. Phys.*, 16, 1081–1104,  
108 <https://doi.org/10.5194/acp-16-1081-2016>, 2016a.

109 Osborne, S.R., Johnson, B.T., Haywood, J.M., Baran, A.J., Harrison, M.A.J., and McConnell, C.L.: Physical and  
110 optical properties of mineral dust aerosol during the Dust and Biomass-burning Experiment, *J. Geophys. Res.*,  
111 113, D00C03, doi:10.1029/2007jd009551, 2008.

112 Ryder, C. L., Highwood, E. J., Rosenberg, P. D., Trembath, J., Brooke, J. K., Bart, M., Dean, A., Crosier, J., Dorsey,  
113 J., Brindley, H., Banks, J., Marsham, J. H., McQuaid, J. B., Sodemann, H., and Washington, R.: Optical  
114 properties of Saharan dust aerosol and contribution from the coarse mode as measured during the Fennec  
115 2011 aircraft campaign, *Atmos. Chem. Phys.*, 13, 303–325, doi:10.5194/acp-13-303-2013, 2013a.

116 von der Weiden, S.-L., Drewnick, F., and Borrmann, S.: Particle Loss Calculator – a new software tool for the  
117 assessment of the performance of aerosol inlet systems, *Atmos. Meas. Tech.*, 2, 479–494, 2009.